PCCP

Accepted Manuscript

ROYAL SOCIETY OF CHEMISTRY

www.rsc.org/pccp

Dynamically Slow Solid-to-Solid Phase Transition Induced by Thermal Treatment on $DimimFeCl_4$ Magnetic Ionic Liquid

Imanol de Pedro, [a]* Oscar Fabelo, [b]* Abel García-Saiz,[a] Oriol Vallcorba, [c] Javier Junquera,[a] Jesús Angel Blanco, [d] João Carlos Waerenborgh, [e] D. Andreica, [f] Andrew Wildes, [b] María Teresa Fernández-Díaz, [b] and Jesús Rodríguez Fernández[a]

[a] CITIMAC, Facultad de Ciencias, Universidad de Cantabria, 39005 Santander.
[b] Institut Laue-Langevin, BP 156X, F-38042 Grenoble Cedex, France.
[c] ALBA Synchrotron Light Source, Cerdanyola del Vallés, Barcelona, Spain.
[d] Departamento de Física, Universidad de Oviedo, 33007 Oviedo, Spain.
[e] Centro de Ciências e Tecnologias Nucleares, Instituto Superior Técnico, Universidade de Lisboa, 2695-066 Bobadela LRS, Portugal
[f] Faculty of Physics, Babes-Bolyai University, 400084 Cluj-Napoca, Romania

ABSTRACT: The results reported here represent the first direct experimental observations supporting the existence of a solid-to-solid phase transition induced by thermal treatment–in Magnetic ionic liquids (MILs). The phase transitions of the solid phases of 1,3-dimethylimidazolium tetrachlorideferrate, $DimimFeCl_4$, are closely related to its thermal history. Two series of solid-to-solid phase transitions can be described in this MIL: (i) from room temperature (RT) phase **II** [space group (s.g.) = $P2_1$] to phase **I-a** [s.g. = $P2_12_12_1$] via thermal quenching or via fast cooling at T > 2K/min; (ii) from phase **I-a** to phase **I-b** [s.g. = $P2_1/c$] when the temperature was kept above 180 K several minutes. The latter one involves a slow translational and reorientational dynamical process of both the imidazolium cation and the tetrachlorideferrate anion and has been characterized using synchrotron and neutron powder diffraction and DFT (density functional theory) studies.

The transition is also connected with the modification of the super-exchange pathways of low-temperature phases which show a global antiferromagnetic behavior. A combination of several experimental methods: magnetometry, Mössbauer and muon spectroscopy together with polarized and non-polarized neutron powder diffraction has been used in order to characterize the different features observed in these phases.

INTRODUCTION

There is increasing scientific effort to design and synthesize ionic liquids (ILs), with novel applications. Ionic Liquids designed for specific tasks can now be found[1]. Examples include use in energy applications such as batteries and ultracapacitors,[2] in the capture of carbon dioxide,[3] and in dissolving cellulose[4]. Magnetic ionic liquids (MILs)[5] are particularly interesting. Owing to their magnetic nature, these compounds have been exploited in a wide range of applications including as magnetic hydraulics in engineering,[6] and as magnetic surfactants.[7]

Despite the quest for new ILs for technical applications, their physical properties are still not fully understood. For example, there is a large research effort and debate as to whether the structure of a molecular liquid can be inferred from its parent solid crystal; i.e. if the mixture and intensity of their intermolecular forces induces a strong association or self-assembly in the liquid state.[8]

To this end, the effect of temperature on the nanostructure of imidazolium ILs has been examined via numerous experimental and theoretical techniques.[8-9] Among them, X-ray scattering experiments[10] and molecular dynamic simulations[11] provide useful information about structural correlations. In the case of MILs, without doubt, there is a large scientific interest to examine the nature and consequences of their ion self-assembly. This is due to the fact that the structural ordering [12] appears to be more pronounced in MILs than in conventional ILs and this has a strong influence on the macroscopic properties of the fluid.[13] Moreover, molecular motion in crystalline solids are also attracting the interest of the scientific community.[14] Materials, such as imidazolium based compounds,[15] that are capable of rotational motion in response to outside driving forces such as light, heat, or electric fields are extremely useful for the development of nanoscale devices or for obtaining new ferroelectric materials.

We have previously performed a preliminary investigation[28] of the thermal properties, (by differential scanning calorimetry) the crystal structure (by neutron powder diffraction and DFT calculations) and of the magnetic properties (by magnetic susceptibility and magnetization measurements) of $DiminFeCl_4$. It showed two solid–solid (s–s) phase transitions, at around 332 and 285 K respectively, upon a fast cooling from above the melting point (348 K). The RT solid phase, labelled as phase **II,** crystallizes in the polar space group $P\,2_1$ (No. 4) with a = 6.5434(2) Å, b = 14.0286(3) Å, c = 6.5314(2) Å, β = 89.921(1)° unit cell and V = 599.55(4) Å^3. The low temperature phase, labelled as **I** (in the present work it is hereafter defined as phase **I-a**) crystallizes in the acentric space group $P2_12_12_1$. (No. 19) with a = 9.1242(1) Å, b = 13.8132(2) Å, c = 9.0359(1) Å, V = 1138.84(2) Å^3 at 10 K. Both unit cell are related by a rotation of 45º

along the monoclinic axis ($a' = a + c$, $b' = b$, $c' = a-c$) plus a translation. Their crystal structures can be described as a succession of organic and inorganic layers extended in the *ab*-plane and stacked along the *b*-axis. The shortest intra-layer Fe-Fe distances is about 6.5 Å; a distance which is notability smaller than the shortest Fe-Fe inter-layer distance (ca 8.2 Å). Although the change of the space group produces changes in the orientation of both the imidazolium counterion and the tetrachlorideferrate anion, the topology of both networks is the same. A detailed descriptions of both crystal structures as well as a tabulated list of the most important crystallographic parameters can be found in ref. 16.

The Phase **I-a** is stable down to 2 K (base temperature) upon fast cooling below the temperature of the solid-to-solid phase transition. The neutron diffraction data show the occurrence of long ranged magnetic order below ca. 3 K. However, all our attempts to determine their magnetic structure were unsuccessful due to the fact that the magnetic reflections were very weak.[16]

In this paper, we connect our preliminary study[16] with the investigation of a new phase, hereafter referred to as **I-b**, obtained after a simple thermal treatment. Phase **I-b** was not observed by differential scanning calorimetry or specific heat using PPMS (see ref 16) neither on cooling nor on warming the sample. In this work after phase I-a was kept for several minutes, phase I-b has appeared and we have determined its crystal structure by combining synchrotron and neutron powder diffraction, corroborated by the results of density functional theory studies. A similar phase transition has been found in 1-Alkyl-3- methylimidazolium Hexafluorophosphate series, $[C_n\text{mim}]PF_6$.[17] revealed by single crystal analysis. This family of compounds has three crystalline polymorphs, namely, the phases α, β □□□ γ. The α phase was the first phase detected from the supercooled liquid stated (177 K), during a heating process around 230 K. The phase α changes to the phase β around 250 K. Finally, the γ phase was obtained from the phase β after the latter was kept for several hours at any temperature betwwen 220 and 280 K.

The main goal of this work is that this transformation obtained by simple thermal treatment is related to changes in the physical properties and macroscopic magnetic interactions of MILs. We have also investigated the mechanism of transformation from phase **I-a** to phase **I-b**. and although both phases show a global antiferromagnetic behavior, a combination of magnetometry, Mössbauer and muon spectroscopy data together with non-polarized and polarized powder neutron diffraction experiments have been needed to shed light on the unusual features observed at low temperature in both phases. Finally, we have used non-polarized neutron diffraction data to determine the magnetic structure of phase **I-b,** which shows similar characteristic to phase **I-a**. Moreover, a remarkable increase in the background at low temperatures has been detected in the non-polarized neutron diffraction analysis. This effect is

much more evident in the phase **I-a**, appearing at a similar temperature range to the onset of long-ranged magnetic ordering, which initially suggests a magnetic source. Polarized neutron diffraction using the *xyz*-polarization analysis technique has been used to understand the origin of this unusual behavior.

RESULTS AND DISCUSSION

Phase transition induced by thermal treatment. Previous X-ray and neutron diffraction data showed that the $DiminFeCl_4$ compound has a structural phase transition from a RT (**II**) to a low temperature phase (**I-a**). In the previous publication, the sample was always cooled down using a "fast" protocol, either using a thermal quenching of the sample in a N_2 flux (down to about 100 K), or within a cryo-stream device for X-ray powder diffraction or placing the sample into a standard orange cryostat, pre-cooled to increase the cooling rate.

An unexpected phase transition from phase **I-a** to phase **I-b** was observed using single-crystal X-ray diffraction (SXRD) as function of the temperature. In this experiment the temperature was varied from 100 to 300 K, at each selected point the temperature was stabilized in order to collect data [Figure S1 (a)]. The occurrence of this phenomenon depends on thermal history. Phase **I-b** could be stabilized from phase **I-a** only when the temperature was kept above 180 K several minutes (Figure S2). From phase **II**, with a cooling rate of circa > 2 K/min, the phase **I-b** was not obtained. It only exhibits a thermo-structural change to phase **I-a** [Figure S1(b)] at similar temperatures to those obtained from DTA data (280 K).[16] For lower cooling rates than 2 K/min from RT, a mixture of both phases (**I-a** and **I-b)** appears sometimes (up to now we could not obtain a pure phase **I-b** by cooling). This is indicative of a decrease of reversibility compared with the warm-up protocol from phase **I-a**. It is worth mentioning that after phase **I-b** is formed, it is stable down to the base temperature and heating further to RT gives phase **II** [Figure S1 (a)] above 260 K [Scheme 1].[16]

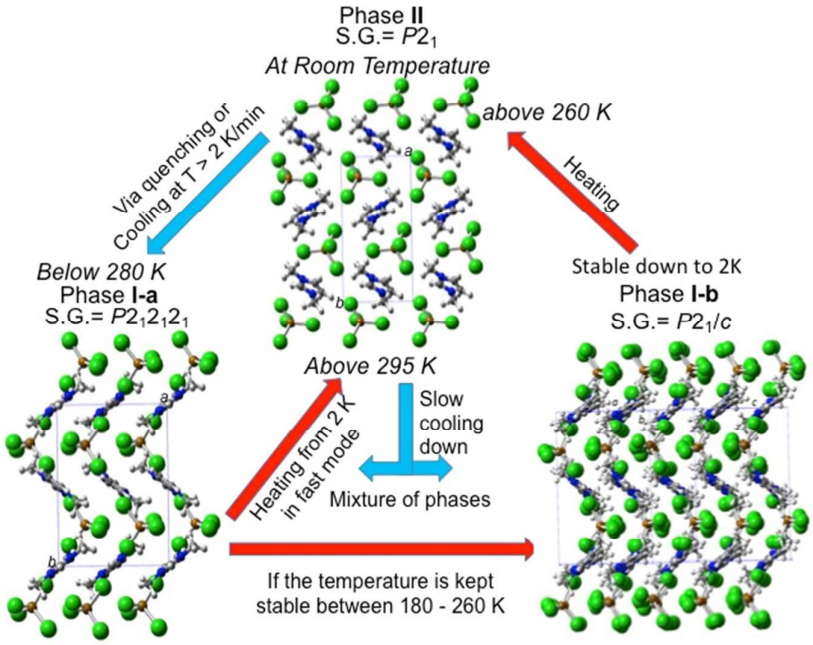

Scheme 1

Crystal Structure Determination. The Rietveld analysis of phase **I-b** was completed using a multipattern approach, combining the synchrotron data with the high-resolution neutron diffraction pattern. The details are presented in the supplementary material. The experimental, calculated and difference powder diffraction profiles are shown in Figure 1 and Figure S3. The final structural parameters and figures of merit for the last refinements are summarized in Tables S1 and S2 and the positional parameters are given in Tables S3, S4 and S5.

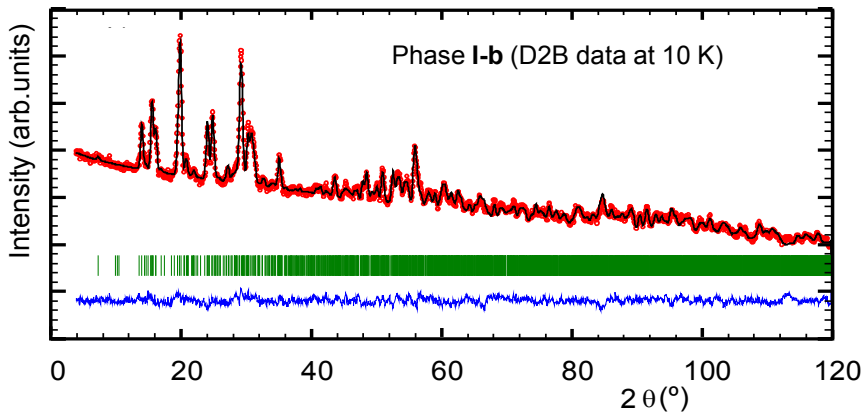

Figure 1. Observed (red points) and calculated (blue solid line) powder diffraction pattern for phase **I-b** of Dimim[$FeCl_4$] at 10 K obtained in the NPD D2B (λ = 1.5938 Å). Positions of the Bragg reflections are represented by vertical bars. The observed-calculated difference patterns are depicted as a blue line in the bottom of the figure.

The phase **I-b** crystallizes in the centrosymmetric monoclinic space group $P2_1/c$ (No. 14) with a = 14.1391(3) Å, b = 13.7039(3) Å, c = 13.2935(3) Å, β = 115.539(2)°, V = 2324(4) Å^3, Z = 2 ρ_{calc} =1.685 g/cm^3, T = 220 K. The crystal structure can be described as a stacking of organic $[Dimim]^+$ and inorganic $[FeCl_4]^-$ layers extended in the *ac*-plane and pillared along the *b*-axis, following a *ABCDABCD* sequence similar to that observed on phases **II** and **I-a**. Each of the *ac*-layers are built up from two independent $[Dimim]^+$ counterions and two $[FeCl_4]^-$ anions. Although the topology of phase **I-b** is the same as that of the other phases,[16] the occurrence of two crystallographically independent cations and anions gives rise to two different orientations of the building blocks. The change of the orientation of the two independent $[FeCl_4]^-$ metal complexes is not very dramatic, and can be seen as a slight rotation with respect to the initial position. The Fe···Fe distances within the *ac*-layer range between 6.27 and 6.57 Å, slightly shorter that those observed in phases **II** and **I-a**. However, the $[FeCl_4]^-$ anions in all phases are fairly regular [mean values of Cl-Fe-Cl bond angles are 109(4)º, 110(3)º and 108(3)º for **II**, **I-a** and **I-b**, respectively] with similar bond lengths [mean values 2.18(6) Å , 2.20(2) Å and 2.21(2) Å].

The $[Dimim]^+$ cations of phase **I-b**, after the phase transition from **I-a**, present a reorientation which involves a non-negligible atomic displacements. The crystal structure of **I-b** displays zig-zag organic-inorganic planes stacked in the [-1, 0, 1] direction whereas for the phase **I-a**, these are extended in the *bc*-plane and pillared along the *a*-axis (see Figure 2). In phase **I-b,** these layers can be described as chains of imidazolium cations extended along the [1, 0, 1] direction and separated by collinear chains of $[FeCl_4]^-$ anions which are extended along the same axis. Within these chains the $[Dimim]^+$ cation has a flip along the *c*-axis with a small distortion along the *a*-direction. This reorientation was not observed in any of the previous phases (**II** and **I-a**).[20] The dihedral angles between the imidazolium ring and the methyl groups [∠ (C-N-C-N)] in all phases range from 177 to 180°. The refined values for the C-C and C-N bond lengths of **I-b** lie in the expected range and are comparable to those found in other imidazolium compounds, as for example in DimimX (X = Cl and Br),[18a] $Bmim_2[XCl_4]$ (X = Fe, Ni and Co)[18b] $EdimimFeX_4$ (X = Cl and Br)[12a] and $EmimFeCl_4$.[19]

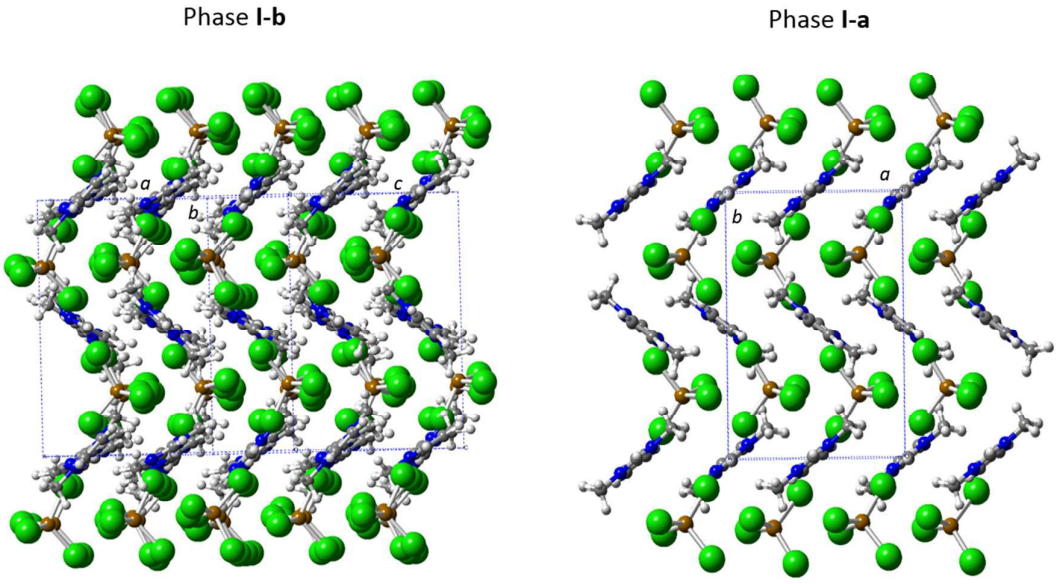

Figure 2. Crystal structures of phase **I-b** and **I-a**. Brown (iron), green (chloride), grey (carbon), blue (nitrogen) and white (hydrogen). The blue dashed square represents the unit cell

Physical Characterization: Magnetometry measurements. The reorientations of the cation and anion groups at the phase transition modifies the super-exchange interactions observed in the phase **I-a**, and therefore the magnetic behavior. In order to unambiguously compare the magnetometry measurements of both phases the magnetic measurements were carried out according to the following thermal treatment: the sample, crystallized in the RT phase (**II**), was quenched to 100 K using the SQUID cryostat in order to obtain the phase **I-a**. The temperature was then cooled to 2 K, in zero field (ZFC) mode. The magnetization of phase **I-a** as a function of applied field was measured at this temperature and 10 K. After that, several low temperature ZFC magnetic susceptibility measurements were performed at different fields from 1 to 50 kOe from 2 to 30 K. The magnetization was then measured as a function of increasing temperature up to 220 K at 1 kOe. This temperature was chosen because is the average temperature of the range where the phase **I-b** was detected in the SXRD data. The sample was kept constant at this temperature for one hour without applying any magnetic field [Neutron diffraction patterns collected using the D1B diffractometer at 220 K as a function of time (Figure S.2) show that phase **I-b** appears after 10 mim] to ensure the transformation of phase **I-a** into phase **I-b**. After this protocol the phase **I-b** should be stabilized at 220K, the temperature was then cooled to 2 K, and the same magnetic measurements as for phase **I-a** were carried out [Figure 3 and S9].

Figure 3 (a) shows the temperature dependence of the molar magnetic susceptibility (χ_m) and inverse susceptibility ($1/\chi_m$) curves of phases **I-a** and **I-b**, measured at 1 kOe after cooling without an applied magnetic field (ZFC). The molar magnetic susceptibilities increase with decreasing temperature up to 3.1 and 5.4 K for phase **I-a** and **I-b** respectively, where a broad

maximum is observed suggesting the existence of a long-ranged magnetic ordering. It disappears in the phase **I-a** for fields higher than 20 kOe, suggesting a partial compensation of the antiferromagnetic interactions. However, the magnetic behaviour as a function of the external magnetic field in the phase **I-b** [see Figure S4 (a)] is slightly different; the maximum of χ_m is shifted to lower temperatures. It is located at 4.15 K for an applied field of 50 kOe, suggesting that the antiferromagnetic interactions remain mainly unchanged [see Figure S4 (b)]. The magnetic data at 1 kOe were fitted in the paramagnetic range using the Curie-Weiss law for S = 5/2 using the molecular field approximation[20]. The least-squares fit of the experimental data from 10 to 220 K is shown in Figure 3 (a). The Curie constant (C) and Curie-Weiss temperature (θ_P), obtained by the fitting, have values of 4.38 and 4.44 emuK/molOe and of -6.9 and -8.5 K, for phase **I-a** and **I-b** respectively, while, the fit gives a value of *zJ,* for **I-a** and **I-b**, of -0.29 and -0.35 K respectively. The values point to weak antiferromagnetic interactions, in accordance with the large distances between iron complex anions (longer than 6.5 Å) and are in agreement with the values previously reported for these types of magnetic pathways.[12, 21]. The Curie constants correspond to an effective paramagnetic moment μ_{eff} = 5.92 and 6.01 μ_B/Fe ion respectively, in good agreement with the expected value of 5.92 μ_B for Fe^{3+} ion with a magnetic spin S = 5/2 and with those found for other paramagnetic compounds based on $[FeCl_4]^-$ ion.[22] Moreover, the temperature dependence of ZFC-FC curves at 10 Oe for each phase does not show any splitting below the broad maxima detected [see inset in Figure 3 (a)], discounting the occurrence of a weak spin-canting or a weak ferromagnetic signal coming from the non-compensation of the different magnetic sites. The possible dynamical response of the magnetic ordering of both phases up to 2 K was discounted by AC magnetic susceptibility measurements (Figure S5).

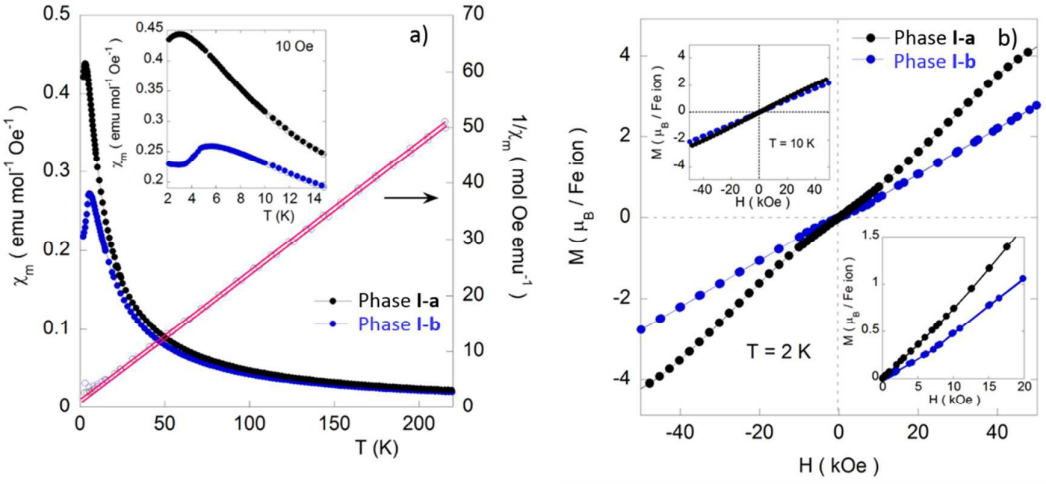

Figure 3. (a) Temperature dependence of χ_m and $1/\chi_m$ for phase **I-a** and **I-b** measured under 1kOe. The solid red line is the fit according to Eq. (1) of the manuscript. The upper inset shows the low temperature ZFC-FC magnetic susceptibility at 10 Oe.(b) Magnetization vs. applied magnetic field at 2 and 10 K (upper inset) for phase **I-a** and **I-b**.

The field dependence of the magnetization for phase **I-a** and **I-b** at 10 K shows a linear behaviour in the whole applied field range confirming the paramagnetic behaviour at this temperature [see upper inset of Figure 3 (b)]. At 2 K, below the Néel temperature of both compounds, the M(H) curves are anhysteretic confirming the absence of a ferromagnetic component. The effective moment value obtained at 50 kOe for the phase **I-a** (4.20 μ_B/Fe ion) is not far from the expected fully-saturated value for a Fe^{3+} ion (5 μ_B/Fe ion). However, after the structural transition to **I-b** the magnetization at 50 kOe is only 2.15 μ_B/Fe ion. This value is far away from the data reported for other MILs based on tetrachloroferrate exhibiting three-dimensional ordering, where the magnetization tends towards saturation for magnetic fields lower than 50 kOe [12a, 23] This feature indicates that, in this system with isotropic exchange interactions [as is expected for Fe(III)], the anisotropy of the magnetic structure plays an important role. Finally, the field dependence of the magnetization of **I-b** displays a small inflection point near 10 kOe, which is correlated with the suppressed drop of magnetic susceptibility measurements for fields higher than 10 kOe. This could be the result of changes to the magnetic structure under the effect of the magnetic field (see description of the magnetic structure).

Mössbauer measurements. The Dimim[$FeCl_4$] sample was cooled at a constant rate of approximately 10 K /minute from room temperature down to 70 K in order to perform a thermal quenching. The spectra of phase **I-a** were then obtained in the range 70-1.9 K. Afterwards, the sample was heated up to 220 K and kept at this temperature for one hour in order to guarantee the occurrence of the solid-to-solid phase transition. After this treatment the sample was cooled down to 70 K and the Mössbauer spectra of phase **I-b** were measured as a function of decreasing temperature.

The Mössbauer spectra of phase **I-a** and **I-b** Dimim[$FeCl_4$] (Figure 4) at 6 K and above consist of a single absorption peak similar to that observed for choline[$FeCl_4$][22] and the analogous tetrahalometallate ionic liquid, Dimim[$FeBr_4$].[12b] The analysis of the spectra reveals that this peak is not adequately fitted by a single Lorentzian line. It consists of a quadrupole doublet with quadrupole splitting (QS) smaller than the line widths of the individual lines (Table S6). This denotes a small electric field gradient at the iron nucleus, and consequently a highly symmetric electric charge distribution around the iron cation with the sp^3 orbitals giving rise to an almost perfect tetrahedral environment. The estimated isomer shifts (IS) relative to metallic Fe at 295 K, IS, for phases **I-a** and **I-b** are equal within experimental error to those of high-spin Fe^{3+} (spin state S = 5/2) in compounds where Fe^{3+} is tetrahedrally coordinated by Cl^- [34, 24] and slightly lower than in $FeCl_3$ where Fe^{3+} has octahedral environment.[25] The fact that no magnetic splittings are observed shows that Fe^{3+} is in a paramagnetic state with $\omega_R >> \omega_L$, where ω_R is

the relaxation frequency of the Fe^{3+} magnetic moments and $\omega_L \sim 10^{-8}$ Hz is the Larmor precession frequency for the ^{57}Fe nucleus.

Below 6 K the spectra depend on the crystallographic phase. Phase **I-a** spectra show that all the Fe^{3+} ions remain in a paramagnetic state down to 2.1 K. Below this temperature, at 1.9 K, a significant broadening of the doublet peaks is observed (Table S6, Figure 4) consistent with a slowing down of ω_R and with the onset of magnetic ordering as was observed by magnetic susceptibility measurements near 3 K. In contrast to the magnetic behaviour of phase **I-a**, **I-b** at 4 K and below displays a well-defined six-peak pattern which implies that ω_R has dropped well below 10^{-8} Hz. The abrupt change in ω_R within a narrow temperature range is typical of the establishment of long-ranged magnetic correlations in the Fe^{3+} sublattice. The sharpness of the transition as well as the narrow peaks observed in the Mössbauer spectra further suggest long-ranged magnetic ordering rather than a spin-glass-like transition. The six-peak patterns observed at 4 K and below are notably not symmetric and two magnetic hyperfine splittings are necessary to fit each spectrum. Both magnetic sextets have equal areas within experimental error (Table S6), in agreement with two different Fe^{3+} magnetic sublattices each containing equal numbers of Fe^{3+}. The quadrupole shifts (2ε) are also different for each sextet. This is related to the occurrence of two different directions for the iron magnetic moments with respect to the crystallographic axes. The temperature dependence of the (2ε) values is shown in Figure S6.

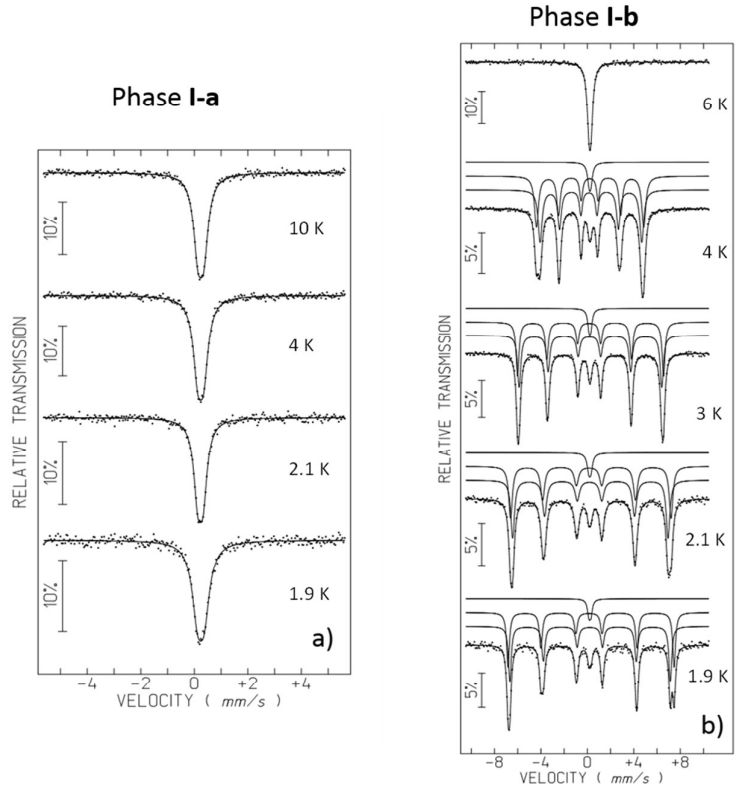

Figure 4. Mössbauer spectra of phases **I-a** and **I-b** collected at different temperatures between 10 and 1.9 K. In phase **I-b** approximately 6% of the Fe^{3+} in the polycrystalline Mössbauer absorber remains paramagnetic probably incorporated in domains with defects at the surface of the small crystal particles.

Muon Spin Spectroscopy (μSR). The μSR experiments were performed in zero applied field in the temperature range 1.6–200 K. The sample was mounted in a special "cup shape" aluminium container covered with a thin layer of mylar tape to prevent leakage. The thermal quenching-heating process was done using a Quantum cryostat following the same experimental protocol as in the Mössbauer measurements.

Low temperature μSR spectra recorded from both phases are shown in Figure 5, along with a comparison between the two. If compared at the same time scale, the runs in the paramagnetic state at 5.2 K are not very different. However, there is a big difference between the first and second cooling process (Observe the different time scale).

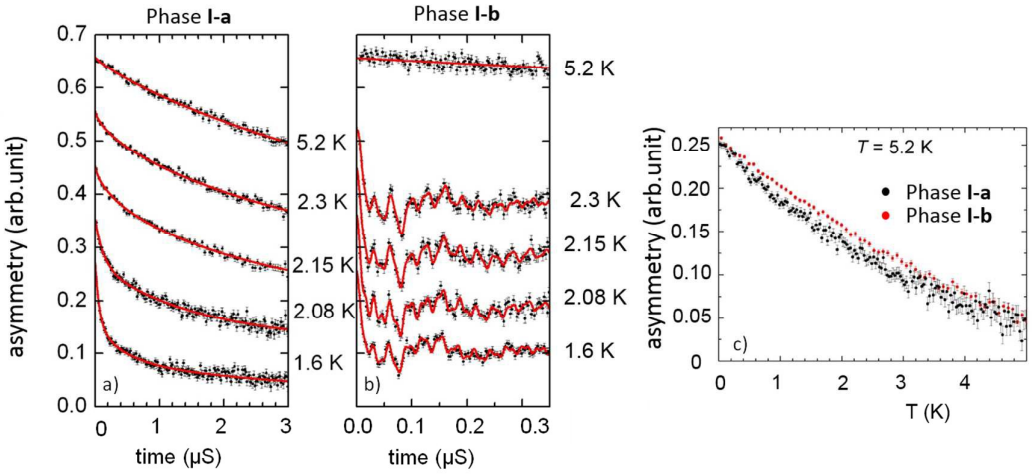

Figure 5. Comparison of spectra recorded and fitted of phase **I-a** (a) and phase **I-b** (b). (c) μSR spectra recorded on two phases at 5.2 K.

The phase **I-a** spectra recorded down to 2.07 K were fitted with a product of a Kubo-Toyabe[26] and a stretched exponential characteristic of a depolarization due to a static field distribution created by the nuclear magnetic moments and a distribution of fluctuation rates of the electronic moments (see Figures S7 and S8):

$$AP(t) = A\left(\frac{1}{3} + \frac{2}{3}\Delta^2 t^2\right) e^{-\frac{\Delta^2 t^2}{2}} e^{-(\lambda t)^{\beta}} \quad (1)$$

where $\beta = 1$ corresponds to a pure exponential relaxation rate while for β = 2, the relaxation rate is Gaussian.

Below 2.07 K, spectra could not be fitted using the same function. Instead, a combination of fast (2/3 term) /slow (1/3 term) relaxing exponentials with an amplitude ratio of about 2/1 was used,

as expected for a magnetic sample: $AP(t)=\left(A_1e^{-\lambda_1 t}+A_2e^{-\lambda_2 t}\right)+A_3e^{-\lambda_3 t}$. The "magnetic part" of the μSR spectra of **I-a** phase could be described by a purely exponential $A_{magn}P_{magn}(t)$, i.e. no oscillations are observed in the μ_{SR} spectra. The fitted parameters up to 1.6 K (see supplementary material and Figures S9 and S10) confirm the onset of a magnetic ordering detected by Mössbauer measurements and suggest that the ordering can not be static below 2K.

In the phase **I-b**, spectra recorded below 5.2 K indicates that the sample becomes magnetic. For example, at 2.3 K one observes clearly that a fast component develops with several oscillations. These spectra were fitted using 4 oscillatory components,

$$AP(t)= A_1e^{-\lambda_1 t}\cos(2\pi\nu_1 t+\varphi_1)+A_2e^{-\lambda_2 t}\cos(2\pi\nu_2 t+\varphi_2)+ \\ +A_3e^{-\lambda_3 t}\cos(2\pi\nu_3 t+\varphi_3)+A_4e^{-\lambda_4 t}\cos(2\pi\nu_4 t+\varphi_4)+A_5e^{-\lambda_5 t}+A_6e^{-\lambda_6 t} \quad (2)$$

which describe the behavior of muons stopped in an interstitial site where they experience a magnetic field (see Figure S.11). For more details of the technique, functions and thermal fitted parameters see the supplementary material.

Magnetic structure determination. In order to determine the magnetic structure of phase **I-b**, we have carried out low temperature neutron diffraction using the high flux D1B diffractometer, working with λ = 2.52 Å. Initially, the sample was milled and placed in a cylindrical vanadium container at room temperature (phase **II**). After that, it was placed inside the orange cryostat at 100 K in order to perform the thermal quenching of the sample (phase **I-a**). Next, the temperature was warmed following a ramp up to 220 K and after waiting 10 min (1 hour in total), the sample **I-a** was completely converted to phase **I-b**. [see Figure S2]. This suggests that the structural transformation occurs when the temperature is stable for enough time to allow the anions to move in the system. After that, the sample with the phase **I-b** structure was cooled down to 1.8 K to collect the neutron diffraction data in the magnetic order phase.

The magnetic ordering of phase **I-a** was previously studied by high flux (D1B with λ = 2.52 Å) and high resolution neutron powder diffraction patterns (D2B with λ = 1.5938 Å). The comparative view of the D1B paramagnetic (10 K) and the magnetically ordered (1.8 K) patterns of phase **I-a** reveals a small sharp Bragg peak (marked with * in Figure 6). This additional elastic intensity is weak, but sufficient to prove the presence of long-ranged antiferromagnetic order. The temperature evolution of the D1B patterns between 1.8 and 10 K [see right inset Figure 6 (a)] shows that the magnetic peaks disappear at temperatures less than around 3 K. Moreover, considerable diffuse scattering is detected for 2θ < 40º, which monotonically increases with decreasing temperature below 9 K. Rietveld refinements above the

magnetic phase transition show that the $P2_12_12_1$ symmetry is maintained from 1.8 to 10 K. Initially, the presence of this unusual behavior was linked to additional magnetic phenomena such as short-ranged magnetic ordering superposed on the long-ranged magnetic order, as observed in other geometrically frustrated antiferromagnetic materials.[27] However, it could arise from other effects such as, nuclear spin-incoherent scattering, random or internal strain.[28] Neutron diffraction with polarization analysis was performed in order to understand the origin of this diffuse scattering (see below).

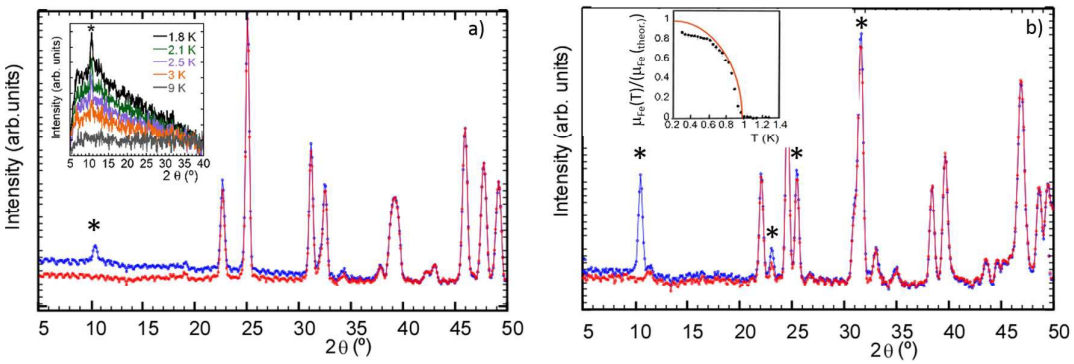

Figure 6. The neutron diffraction profiles of phase **I-a** (a) and **I-b** (b) at 10 (red) and 1.8 K (blue) obtained in D1B. The (*) dots show the magnetic contributions. [left inset (a)] Temperature dependence of the difference diagrams of D1B patterns between 1.8 and 9 K which have been obtained subtracting the nuclear contribution (pattern at 10 K). [Right inset (b)] The temperature dependence of the normalized Fe^{3+} magnetic moment (calculated from $\mu_{Fe}(T)/\mu_{Fe}$, the μ_{Fe} being the theoretical value of ca. 5 μ_B) obtained from the fit of the neutron diffraction pattern and the expected theoretical dependence for the Brillouin function with S = 5/2 (red line).

The comparison of patterns measured in the paramagnetic (10 K) and the magnetically ordered (1.8 K) [Figure 6 (b)] regimes for phase **I-b** revealed the occurrence of several well defined magnetic peaks. The temperature evolution of the neutron diffraction pattern places the onset of a magnetic ordering around $T_N = 5.5$ K. Moreover, the diffuse scattering almost disappears, showing a significant difference between the phases **I-a** and **I-b**. Focusing on the ordered magnetic structure of phase **I-b** (phase **I-a** does not show enough magnetic peaks to propose a realistic magnetic model), below T_N, the magnetic reflections can be indexed with the propagation vector **k** = (0, 0, 0), indicating that the magnetic and nuclear symmetry is the same. Details of the magnetic structure calculation using Bertaut's symmetry analysis method [29] are described in supplementary material and in Table S7.

The magnetic model obtained has ferromagnetic layers, extended into the *ac*-plane, which are antiferromagnetically coupled along the *b*-axis with a possible canting that would produce a global ferromagnetic behavior. According to magnetometry data, the occurrence of any canting

is discounted. Moreover, Mössbauer data display six peaks in the patterns below Néel temperature which are not symmetrical (two magnetic hyperfine splittings are necessary to fit each spectrum). Therefore, the magnetic structure of phase **I-b** should have two Fe^{3+} magnetic sublattices with different magnetization directions relative to the crystallographic axes. Subsequently, the relative orientation of the magnetic moments of both symmetry-related magnetic sites present in this phase were refined. The best fitting of the D1B data at 1.8 K gives for iron $Fe(1)^{3+}$ sublattice R_{tetha}= 176º(5) and for $Fe(2)^{3+}$ R_{tetha}= 140º(10) in good agreement with the Rietveld refinement of the D2B data at 2 K. The refined magnetic moment for both Fe^{3+} magnetic sublattices have been constrained to be equal, giving a refined value of 4.64(1) μ_B; lower than the expected value of 5 μ_B for Fe^{3+} in high-spin configuration due to the fact that the spin density is not strictly localized on the iron ions, but is partially delocalized onto the chloride atoms of the metal complex ion [16] (see details in theoretical calculations). In order to avoid overparameterization and due to the negligible value obtained in the first refinements, the magnetic moment component along the *b* axis (ϕ angle, in spherical coordinates) was kept equal to zero, giving rise to a collinear antiferromagnetic behavior which is in good agreement with the macroscopic magnetic measurements. The final refinements are shown in Figure S12 of Supplementary Material and the corresponding magnetic structure is shown in Figure 7. The nuclear and magnetic discrepancy factors are R_p = 22.6 % and 12.4 %, R_{wp} = 15.7 % and 12.1 %, R_{Bragg} = 11.9 % and 5.8 % and R_{mag} = 8.7 % and 6.8 % for D1B and D2B data respectively. Finally, sequential refinements of D1B between 1.8 and 10 K were performed using the FullProf suite[30] in order to follow the temperature dependence of the modulus of the Fe^{3+} magnetic moment, μ_{Fe}. The right inset of Figure 6 (b) displays this evolution with the theoretical dependence corresponding to a Brillouin function with S = 5/2.[31]

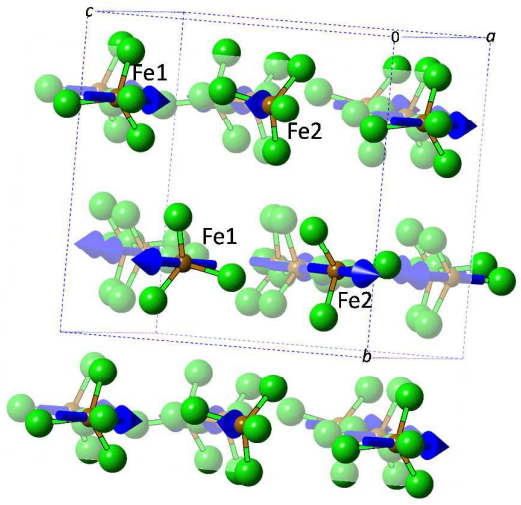

Figure 7. Magnetic structure of phase **I-b** at 1.8 K. The Dimim counterions have been omitted for the sake of clarity.

Neutron polarization analysis. The same thermal history process as that for the previous non-polarized neutron measurements was used for the *xyz*-polarization analysis experiment on the D7 diffractometer. The temperature evolution of the total cross section of phase **I-a** between 1.5 and 15 K is shown in Figure 8 (up-left). The separated magnetic cross sections displays three peaks at temperatures below 3 K. The separation worked well and the statistics are good despite the very large incoherent scattering signal due to the presence of 13 H atoms in the organic part of $DimimFeCl_4$ sample. The successful separation of the magnetic contribution was confirmed checking that the sample does not have preferred orientation and hence the component of the magnetization perpendicular to the scattering vector is isotropic. After thermal stabilization, phase **I-b** [Figure 8 (up-right)] shows the same number of magnetic reflections, in the same Q positions, but now these disappear at temperatures lower that 6 K. This result allows us to propose that both magnetic structures could be similar with stronger magnetic couplings in phase **I-b**. The first magnetic reflection located at Q = 0.47 $Å^{-1}$ at 1.5 K, displays an intensity almost twice as high in phase **I-b** as that in phase **I-a**, which should be related with the modification of the super-exchange interactions after the nuclear phase transition.

At 1.5 K, the nuclear spin-incoherent cross section of phase **I-a** increases monotonically for Q < 1.4 $Å^{-1}$ [Figure 8 (centre-left)]. Moreover, the intensity at the lowest Q drops by about 10% as temperature increases up to 10 K. A similar behaviour is found for the phase **I-b** but now its intensity increases less than 5% from 10 to 1.5 K. This issue confirms that the increase of background at low temperature detected with non-polarized neutron diffraction data (D2B and D1B) has no magnetic origin (inelastic magnetic background). However, the cooling-heating process for the two phases causes a significant difference in the diffuse scattering. As far as we know is the first time that this behaviour is observed in molecular-based material. Our hypothesis is that this behavior could arise from the hydrogen atoms which are the dominant contributers to the nuclear spin-incoherence term. The presence of correlations between neighboring atoms (short-ranged order) is discounted since this would give rise to nuclear coherent scattering (see Figure S13).[32] A logical explanation for this temperature dependence is that there is strong incoherent inelastic scattering. Therefore quasielastic neutron scattering (QENS) and inelastic neutron scattering (INS) data will be obtained to give us more detail about this unusual behavior.

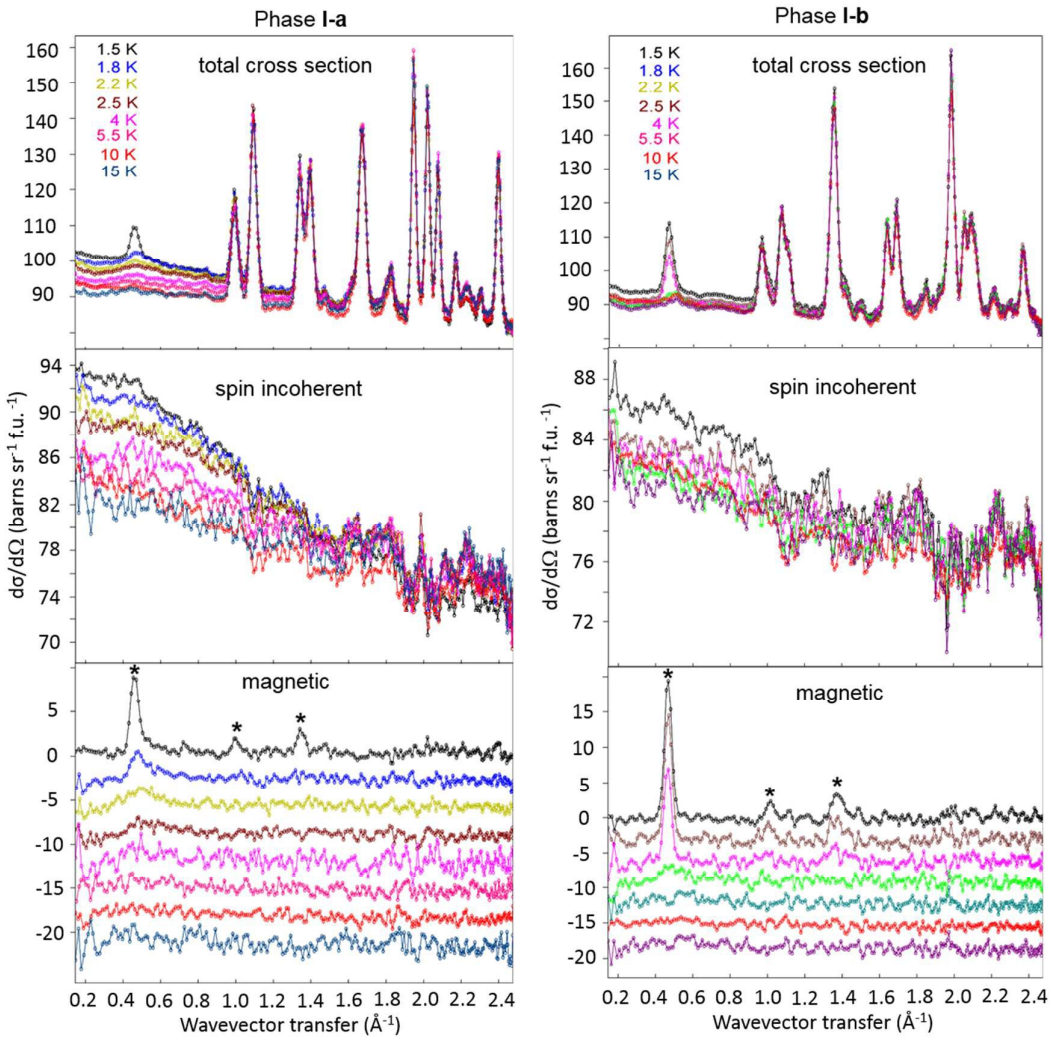

Figure. 8. Separation of nuclear and spin incoherent magnetic (The patterns have been shifted 2 barns sr^{-1} $f.u.^{-1}$ for clarity) from the total neutron scattering cross sections of phase **I-a** (left) phase **I-b** (right) measured using *xyz*-polarization analysis on D7 at several temperatures between 1.5 and 15 K. The (*) dots show the magnetic peaks.

Density functional theory calculations. The crystal and magnetic structures of phase **I-a** and **I-b** were also investigated by *ab initio* calculations. Density functional theory (DFT), performed using the SIESTA[33] code, was employed as it offers an efficient and accurate quantum mechanical method to optimize crystal structures, to calculate the equilibrium energies, to obtain the charge distributions and to predict van der Waals (vdW) interactions in the DFT context. It was used with a formalism to deal with vdW interactions, which have been successfully applied to the study of ILs[34].

We carried out a structural relaxation of phase **I-a**[16] and **I-b** to refine the atomic coordinates starting from the experimental coordinates obtained by the D2B Rietveld analysis at 10 K (Table S.8). The intramolecular geometries (reduced coordinates) and distances between

$[Dimim]^+$ cation and $[FeCl_4]^-$ anion gained by DFT are not too far away from the starting point, with only an underestimation of 3% relative to the experimental data, within the standard deviations of the functional approach.[35] We determined the E_0 of phase **I-b**, which represents the energy per atom of the compound under investigation in its ground state i.e. at 0 K and without external stress, to be 37 meV/84 atoms which is more stable than the phase **I-a**. Therefore, we confirm that after the solid-to-solid transition the crystal structure (**I-b**) is more stable. We also checked the existence of attractive anion-π interactions[36] using the projected density of states (PDOS) of the imidazolium with the chloride of the metal complex anion (see Figure S14 of supplementary material). Figure 9 displays how the wave function can connect Fe(1) and Fe(2) atoms from layer to layer across the π orbital of the imidazolium ring. Thus, an electronic transmitting mechanism can be propagated via anion-π interactions, the anion residing above the ring centroid, which is characteristic of strong anion-π interactions.[37]

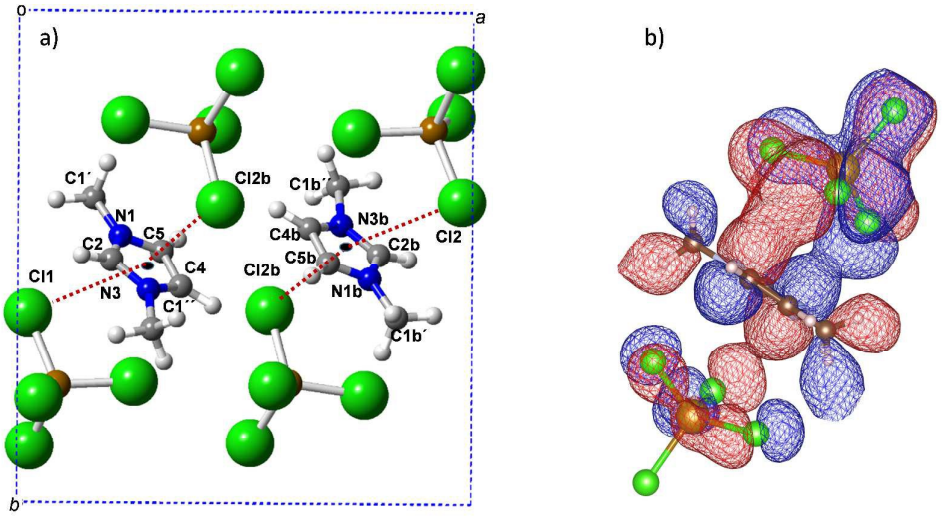

Figure 9 (a). Shorter π−d interaction distances between the metal complex and imidazolium centroid. Relevant distances and orientations are display in Table 2 which show potential anion–π interactions between on imidazolium and tetrachlorideferrate ions in phase **I-b** according IUPAC recommendation. **(b):** Representation of the wave function for the state with energy of −2.34 eV below the Fermi energy, where there is orbital overlapping (red and blue colors represent the positive and negative part, respectively).

We checked the stability of the proposed antiferromagnetic structure of phase **I-b** with respect to the other three possible magnetic configurations allowed in this space group. The calculations display the lowest energy for this configuration, in good agreement with the result obtained by the neutron experimental data. The sum of the Mulliken populations obtained gives a value of 4.98 μ_B, which is expected for a Fe^{+3} with a high spin of S=5/2.[16] The quantity of spin transferred to one chloride atoms is 0.26 μ_B, the total transfer being 1.04 μ_B, which represents

about 21 % of the magnetic moment. These numbers are consistent with a direct integration of the charge density over spheres surrounding atoms, assuming non-overlapping spheres around Fe and Cl of 2.4 Bohr magnetons. Comparing the present result with that obtained for phase **I-a**, we determine that the delocalization is similar (total spin density transfer from Fe to Cl = 1.06 μ_B),[16] being also in good agreement with the data reported in other Fe^{+3} materials.[38]

Magneto-structural correlations. For the magneto-structural discussion, the crystal structure at 10 K (high resolution neutron powder diffraction) will be taken due to the better determination of atomic positions relevant for the magnetic ordering. A comparison of the most relevant interatomic distances of phases **I-a** and **I-b** is displayed in Table 1 and 2. The data obtained from synchrotron powder diffraction are shown in Table S9.

On comparing the structural features of both phases, direct Fe···Fe interactions are not present due to the Fe···Fe distances being between 6.16 and 8.16 Å (see Table 2). Therefore, direct super-exchange anion−anion interactions (Fe−Cl···Cl−Fe) mediate magnetic couplings between an iron ion and its first shell of neighbouring iron ions. In addition, phase **I-b**, in agreement with the DFT calculations should also display indirect super-exchange anion−anion interactions through anion-π interactions (Fe−Cl···Im···Cl− Fe), where Im represents an imidazolium donor cation (see Table 1).

Figure 10 displays a comparative view of the possible super-exchange anion−anion interactions projected on the *ac*-plane on phases **I-a** and **I-b** according to the most appropriate model of the magnetic structure obtained from neutron diffraction data. The strength of these super-exchange anion−anion interactions of both phases, (Fe−Cl···Cl−Fe), can be qualitatively compared by noting that shorter Cl···Cl distances, larger Fe−Cl···Cl angles, and torsion angles near 0 and 180° are correlated with stronger magnetic exchange constants.[39] Two intraplane interactions, $J_\perp$, defined by J_1 and J_2, connect the iron atoms in linear chains in the *ac*-plane on both phases. The phase **I-a** shows Cl···Cl distances of 3.603 and 3.564 Å for J_1 and J_2, values which are smaller than the sum of the vdW radii of two chloride atoms (3.70 Å), having remarkable agreement with other reported magnetic coupling lengths in several metal−organic materials.[40] For the phase **I-b**, some of these distances are longer, ranging from 3.601 to 4.064 Å. Moreover, for phase **I-a** the four chlorine atoms involved in the exchange coupling pathways present two well-separated ranges of super-exchange angles: (i) Fe−Cl···Cl, with 157.1 and 158.5° and (ii) Cl···Cl−Fe, with 87.8 to 95.8° and τ of 155.2 and 171.3° for J_1 and J_2, respectively. These parameters are nearly maintained after the phase transition to phase **I-b** where Fe−Cl···Cl, which range between 130.3 and 164.4° and Cl···Cl−Fe, varying from 82.8 to 164.4° with τ ranging from 149.8 to 179.3°. According to the magnetic structure obtained, these types of magnetic coupling should promote ferromagnetic interactions.

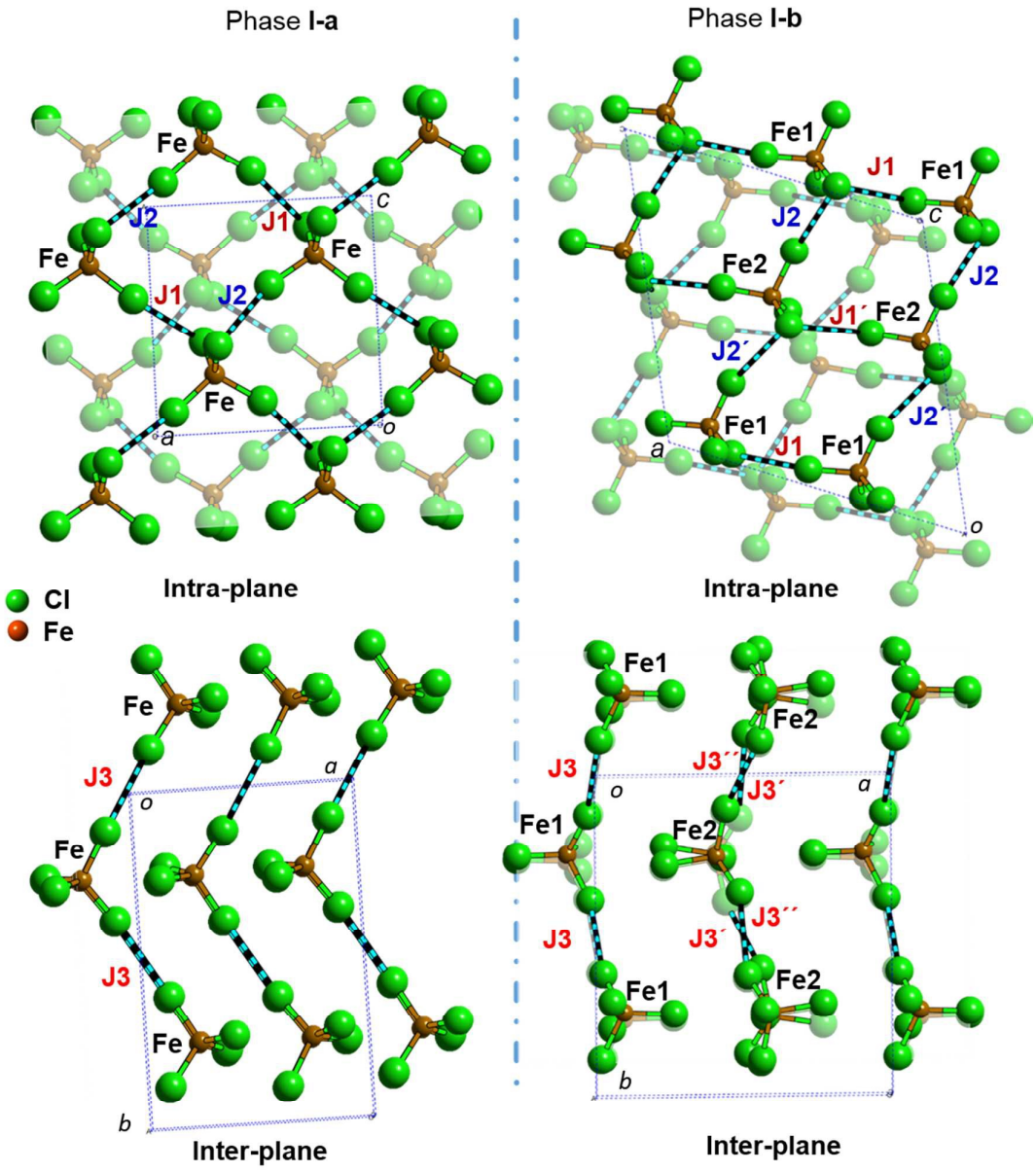

Figure 10. Schematic view of the possible intra and inter-plane magnetic exchange pathways for phase **I-a** and **I-b** via Fe−Cl···Cl−Fe bridge

The J_3 interaction, $J_\perp$ or interplane super-exchange magnetic coupling, gives rise to zigzag chains creating a ladder structure that is aligned parallel to the *b* direction [Figure 10]. This is the strongest coupling, according to the predominant antiferromagnetic behaviour of both phases. The Cl···Cl distance, in phase **I-a**, have a value of 3.770 Å. After the solid-transition, these lengths are slightly modified to vary from 3.435 to 3.770 Å for the Fe(1)-Cl···Cl-Fe(1) (J_3) or for Fe(2)-Cl···Cl-Fe(2) (J_3' and J_3'') exchange coupling [see right picture of Figure 10 (b)]. The Fe−Cl···Cl and Cl···Cl−Fe angles on phase **I-a** (J_3) show a values of 170.6 and 173.5° with τ of 14.35° while in phase **I-b**, Fe−Cl···Cl ranges from 148.0 to 156.5°, and Cl···Cl−Fe

varies between 148 to 165.5° with τ from 120.5 to 180.0°. The analysis of these parameters reveals the reason why the strength of these super-exchange anion−anion interactions (Fe−Cl···Cl−Fe) can be larger within phase **I-b**. The main factor should be attributed to shorter Cl···Cl distances which are correlated with stronger magnetic exchange constants. Moreover, it should be taken into consideration that phase **I-b** could also have indirect super-exchange antiferromagnetic interactions through anion-π pathways (Fe−Cl···Im···Cl− Fe) between adjacent planes.

Conclusions

In the present work we have shown how the application of a thermal treatment can induce a solid-to-solid phase transition in the $DimimFeCl_4$ MIL. The solid phase of $DimimFeCl_4$, after a thermal quenching, (phase **I-a**) crystallizes in the orthorhombic structure with a three-dimensional antiferromagnetic ordering below 3 K. After a thermal treatment of phase **I-a**, a crystal structure transformation to a monoclinic phase takes place, involving a translational and reorientational process of the Dimim counterions and $[FeCl_4]^-$ anions. This feature is connected with the modification of the super-exchange pathways after the solid-to-solid phase transition which increases the magnetic long-ranged order temperature, T_N from ca. 3 to 5.4 K. The magnetic structure formed can be described as antiferromagnetic layers pillared along the *b*-axis. Using polarized neutron diffraction we have studied the origin of the increase of the background detected below 9 K for both phases. The results unambiguously show that this signal has no magnetic origin and therefore should probably be associated with the hydrogen atoms.

The cooling rate could be a very important variable for the dynamical process, structural transformations and magnetic properties of MILs. This observation could pave the way towards novel stimuli-responsive materials using temperature effects. Similar trends are expected in ILs in which bulky cations exhibit a strong electrostatic coupling with small anions, such as halides.

ASSOCIATED CONTENT

*Supporting Information

Supporing information contains Experimental details of high-resolution synchrotron X-ray diffraction, Neutron non-polarization and polarization diffraction experiments, magnetic and Mössbauer measurements, muon spin relaxation (μSR) spectroscopy data, DFT calculations with computational details. Crystallographic information (CIF data) of phases **II**, **I-a** and **I-b**

and can be obtained free of charge from The Cambridge Crystallographic Data Centre via www.ccdc.cam.ac.uk/ data_request/cif.

This material is available free of charge via the Internet.

AUTHOR INFORMATION

Corresponding Authors: depedrovm@unican.es; fabelo@ill.fr

Notes

The authors declare no competing financial interest.

ACKNOWLEDGMENTS

Financial support from the Spanish Ministerio de Ciencia e Innovación (Project MAT2014-55049-R, MAT2014-5611-2-R, and FC-15-GRUPIN14-037), the Romanian UEFISCDI (Project PN-II-ID-PCE-2011-3-0583 (85/2011), and Becas Iberoamericas Jóvenes Profesores Investigadores, 2011, Santander Universidades is acknowledged. C^2TN/IST author gratefully acknowledges the FCT (Portugal) support through the UID/Multi/04349/2013 project. The authors also gratefully acknowledge the computer resources, technical expertise, and assistance provided by the Red Española de Supercomputación. The paper is partly based on the results of experiments carried out at Paul Scherrer Institut (PSI), Villigen, Switzerland, ALBA synchrotron light source in Barcelona and Institute Laue-Langevin (ILL) in Grenoble.

Keywords: Magnetic Ionic Liquids; Solid-to-Solid Phase Transition, Three-Dimensional Magnetic Ordering; Thermal Treatment, Neutron diffraction.

REFERENCES

[1] a) R. Giernoth, *Angew. Chem. Int. Ed.* **2010**, *49*, 2834-2839; b) E. D. Bates, R. D. Mayton, I. Ntai and J. H. Davis, *JACS* **2002**, *124*, 926-927; c) S.-g. Lee, *Chem. Comm.* **2006**, 1049-1063; d) Z. Zhang, Y. Xie, W. Li, S. Hu, J. Song, T. Jiang and B. Han, *Angew. Chem. Int. Ed.* **2008**, *47*, 1127-1129; e) S. Tang, G. A. Baker and H. Zhao, *Chem. Soc. Rev.* **2012**, *41*, 4030-4066.

[2] a) A. Lewandowski and A. Świderska-Mocek, *J. Power Sources* **2009**, *194*, 601-609; b) K. Xu, *Chem. Rev.* **2004**, *104*, 4303-4418; c) P. Simon and Y. Gogotsi, *Nature materials* **2008**, *7*, 845-854; d) M.-C. Lin, M. Gong, B. Lu, Y. Wu, D.-Y. Wang, M. Guan, M. Angell, C. Chen, J. Yang and B.-J. Hwang, *Nature* **2015,** 520(7547), 324-328.

[3] a) X. Huang, C. J. Margulis, Y. Li and B. J. Berne, *JACS* **2005**, *127*, 17842-17851; b) B. E. Gurkan, J. C. de la Fuente, E. M. Mindrup, L. E. Ficke, B. F. Goodrich, E. A. Price, W. F. Schneider and J. F. Brennecke, *JACS* **2010**, *132*, 2116-2117.

[4] a) R. P. Swatloski, S. K. Spear, J. D. Holbrey and R. D. Rogers, *JACS* **2002**, *124*, 4974-4975; b) A. M. Socha, R. Parthasarathi, J. Shi, S. Pattathil, D. Whyte, M. Bergeron, A. George, K. Tran, V. Stavila and S. Venkatachalam, *Proc. Natl. Acad. Sci.***2014**, *111*, E3587-E3595.

[5] A. Branco, L. C. Branco and F. Pina, *Chem. Comm.* **2011**, *47*, 2300-2302.

[6] P. Scovazzo, C. A. M. Portugal, A. A. Rosatella, C. A. M. Afonso and J. G. Crespo, *J. Colloid and Interface Sci.***2014**, *428*, 16-23.

[7] P. Brown, A. Bushmelev, C. P. Butts, J. Cheng, J. Eastoe, I. Grillo, R. K. Heenan and A. M. Schmidt, *Angew. Chem. Int. Ed.* **2012**, *51*, 2414-2416.
[8] R. Hayes, G. G. Warr and R. Atkin, *Chem. Rev.* **2015**, *115*, 6357-6426.
[9] S. M. Urahata and M. C. Ribeiro, *J. Chem.Phys.* **2004**, *120*, 1855-1863.
[10] A. Triolo, O. Russina, H.-J. Bleif and E. Di Cola, *The J. Chem.Phys. B* **2007**, *111*, 4641-4644.
[11] E. Bodo, L. Gontrani, R. Caminiti, N. V. Plechkova, K. R. Seddon and A. Triolo, *J. Chem.Phys. B* **2010**, *114*, 16398-16407.
[12] a) A. García-Saiz, I. de Pedro, O. Vallcorba, P. Migowski, I. Hernández, L. F. Barquin, I. Abrahams, M. Motevalli, J. Dupont and J. A. Gonzalez, *RSC Adv.* **2015**, *5*, 60835-60848; b) A. Garcia-Saiz, I. de Pedro, P. Migowski, O. Vallcorba, J. Junquera, J. A. Blanco, O. Fabelo, D. Sheptyakov, J. C. Waerenborgh, M. T. Fernandez-Diaz, J. Rius, J. Dupont, J. A. Gonzalez and J. R. Fernandez, *Inorg. Chem.* **2014**, *53*, 8384-8396.
[13] C. E. S. Bernardes, T. Mochida and J. N. Canongia Lopes, *Phys. Chem. Chem. Phys.* **2015**, *17*, 10200-10208.
[14] a) J. Harada, M. Ohtani, Y. Takahashi and T. Inabe, *JACS* **2015**, *137*, 4477-4486; b) J. M. Abendroth, O. S. Bushuyev, P. S. Weiss and C. J. Barrett, *ACS nano* **2015**, *9*, 7746-7768.
[15] a) X. Zhang, X.-D. Shao, S.-C. Li, Y. Cai, Y.-F. Yao, R.-G. Xiong and W. Zhang, *Chem. Comm.* **2015**, *51*, 4568-4571; b) Z. Sun, T. Chen, J. Luo and M. Hong, *Angew. Chem. Int. Ed.* **2012**, *51*, 3871-3876.
[16] A. García-Saiz, P. Migowski, O. Vallcorba, J. Junquera, J. A. Blanco, J. A. González, M. T. Fernández-Díaz, J. Rius, J. Dupont, J. Rodríguez Fernández and I. de Pedro, *Chem. Eur. J.* **2014**, *20*, 72-76.
[17] T. Endo, H. Masu, K. Fujii, T. Morita, H. Seki, S. Sen, K. Nishikawa, K, *Cryst. Growth Des.* **2013**, *13(12)*, 5383-5390.
[18] a) I. de Pedro, A. García-Saiz, J. Dupont, P. Migowski, O. Vallcorba, J. Junquera, J. Rius and J. Rodríguez Fernández, *Cryst. Growth Des.* **2015**, *15*, 5207-5212. b) C. Zhong, T. Sasaki, A. Jimbo-Kobayashi, E. Fujiwara, A. Kobayashi, M. Tada and Y. Iwasawa, *Bull. Chem. Soc. Jpn.***2007**, *80*, 2365-2374.
[19] T. Bäcker, O. Breunig, M. Valldor, K. Merz, V. Vasylyeva and A.-V. Mudring, *Cryst. Growth Des.* **2011**, *11*, 2564-2571.
[20] R. Boca, *A Handbook of Magnetochemical Formulae*, Elsevier, **2012**, p. 1010.
[21] J. A. Zora, K. R. Seddon, P. B. Hitchcock, C. B. Lowe, D. P. Shum and R. L. Carlin, *Inor. Chem.* **1990**, *29*, 3302-3308.
[22] I. de Pedro, A. Garcia Saiz, J. A. Gonzalez, I. Ruiz de Larramendi, T. Rojo, C. Afonso, S. Simeonov, J. C. Waerenborgh, J. A. Blanco and J. Rogriguez, *Phys. Chem. Chem. Phys.* **2013,** 15,12724-1280.
[23] a) I. de Pedro, D. P. Rojas, J. Albo, P. Luis, A. Irabien, J. A. Blanco and J. Rodriguez Fernandez, *Journal of Physics-Condensed Matter* **2010**, *22*; 296006-296010 b) I. de Pedro, D. P. Rojas, J. A. Blanco and J. Rodriguez Fernandez, *J. Magn. Magn. Mater.* **2011**, *323*, 1254-1257.
[24] a) J. Briers, W. Eevers, M. De Wit, H. J. Geise, J. Wauters, M. Van Bavel, H. Bemelmans and G. Langouche, *The J. Chem.Phys.* **1995**, *99*, 12971-12974; b) J. C. Waerenborgh, S. Rabaça, M. Almeida, E. B. Lopes, A. Kobayashi, B. Zhou and J. S. Brooks, *Phys.Rev.B* **2010**, *81*, 060413.
[25] N. N. Greenwood and T. C. Gibb, *Mössbauer spectroscopy*, Chapman and Hall London, **1971**, p2450.
[26] R. Hayano, Y. Uemura, J. Imazato, N. Nishida, T. Yamazaki and R. Kubo, *Phys. Rev. B* **1979**, *20*, 850.
[27] a) O. A. Petrenko, C. Ritter, M. Yethiraj and D. McK Paul, *Physical Review Letters* **1998**, *80*, 4570-4573; b) J. E. Greedan, C. R. Wiebe, A. S. Wills and J. R. Stewart, *Phys. Rev.B* **2002**, *65*, 184424.
[28] J. Stewart, P. Deen, K. Andersen, H. Schober, J.-F. Barthélémy, J. Hillier, A. Murani, T. Hayes and B. Lindenau, *J. Appl. Crystal.* **2009**, *42*, 69-84.
[29] E. Bertaut, *Acta Crystall. Sect. A* **1968**, *24*, 217-231.
[30] J. Rodríguez-Carvajal, *J. Appl. Crystallogr. 14 (1981) 149*.

[31] J. A. Blanco, J. I. Espeso, J. García Soldevilla, J. C. Gómez Sal, M. R. Ibarra, C. Marquina and H. E. Fischer, *Phys. Rev. B* **1999**, *59*, 512-518.
[32] M. De Vries, J. Stewart, P. Deen, J. Piatek, G. Nilsen, H. Rønnow and A. Harrison, *Phys.Rev. Lettl* **2009**, *103*, 237201.
[33] J. M. Soler, E. Artacho, J. D. Gale, A. García, J. Junquera, P. Ordejón and D. Sánchez-Portal, *J. Phys. Condens.Matter* **2002**, *14*, 2745-2779.
[34] M. G. Del Pópolo, R. M. Lynden-Bell and J. Kohanoff, *J. Chem.Phys. B* **2005**, *109*, 5895-5902.
[35] M. Dion, H. Rydberg, E. Schröder, D. C. Langreth and B. I. Lundqvist, *Phys. Rev. Lett.* **2004**, *92*, 246401.
[36] B. L. Schottel, H. T. Chifotides and K. R. Dunbar, *Chem. Soc. Rev.* **2008**, *37*, 68-83.
[37] L. M. Salonen, M. Ellermann and F. Diederich, *Angew. Chem. Int. Ed.* **2011**, *50*, 4808-4842.
[38] J. Campo, J. Luzón, F. Palacio, G. J. McIntyre, A. Millán and A. R. Wildes, *Phys. Rev. B* **2008**, *78*, 054415.
[39] R. Bertani, P. Sgarbossa, A. Venzo, F. Lelj, M. Amati, G. Resnati, T. Pilati, P. Metrangolo and G. Terraneo, *Coord. Chem. Rev.* **2010**, *254*, 677-695.
[40] M. M. Turnbull, C. P. Landee and B. M. Wells, *Coord. Chem. Rev.* **2005**, *249*, 2567-2576.

Table 1. Interatomic distances between the imidazolium and the metal complex anion in the crystal structures of phases **I-a** and **I-b** at 10 K obtained from Rietveld refinements of the high resolution neutron powder diffraction data.

$[FeCl]^-\cdots[Dimim]^+$ (potential π-d interactions)		
Phase **I-a**		
	length (Å)	angle (º)
Fe(1)-Cl(1)···centroid(1)	3.904(8)	81.5(3)
Fe(1)-Cl(3)···centroid(1)	3.907(9)	80.7(3)
Phase **I-b**		
Fe(1)-Cl(2)···centroid(1)	3.88(2)	81.6(7)
Fe(1)-Cl(1)···centroid(2)	3.61(2)	89.9(8)
Fe(2)-Cl(2b)···centroid(1)	3.56(2)	88.6(8)
Fe(2)-Cl(2b)···centroid(2)	3.67(2)	93.1(8)

Table 2. Selected geometrical parameters, bond lengths (Å) and angles (deg) obtained from high-resolution neutron diffraction (experiment at 10 K) related to the possible magnetic exchange pathways for phase **I-a** and **I-b**.

	Intra-plane						
	Magnetic exchange Pathways	**Direct distance Fe-Fe/Å**	**Bond/Å Cl-Cl**	**Angle/° Fe-Cl-Cl**	**Angle/° Cl-Cl-Fe**	**Torsion angle (τ)/º**	**Direction**
Phase **I-a**	**J1**	6.623	3.603	158.50	95.82	171.32	*ac*/**F**
	J2	6.162	3.564	157.06	87.75	155.16	*ac*/**F**
Phase **I-b**	**J1** ***(Fe1-Fe1)***	6.571	4.064	130.31	88.08	144.75	*ac*/**F**
	J1´ ***(Fe2-Fe2)***	6.566	3.858	150.09	91.15	152.91	*ac*/**F**
	J2 ***(Fe1-Fe2)***	6.270	3.601	164.42	85.81	162.43	*ac*/**F**
	J2´ ***(Fe2-Fe1)***	6.336	3.914	149.99	82.80	179.30	*ac*/**F**
	Inter-plane						
	Magnetic exchange Pathways	**Direct distance Fe-Fe/Å**	**Bond/Å Cl-Cl**	**Angle/° Fe-Cl-Cl**	**Angle/° Cl-Cl-Fe**	**Torsion angle (τ)/º**	**Direction /Type**
Phase **I-a**	**J3**	8.164	3.765	170.6	173.5	14.35	*b*/**AF**
Phase **I-b**	**J3** ***(Fe1-Fe1)***	8.092	3.767	156.22	164.51	120.45	*b*/**AF**
	J3´ ***(Fe2-Fe2)***	7.843	3.435	166.48	165.48	180.00	*b*/**AF**
	J3´´ ***(Fe2-Fe2)***	7.581	3.630	147.97	147.96	180.00	*b*/**AF**

TOC

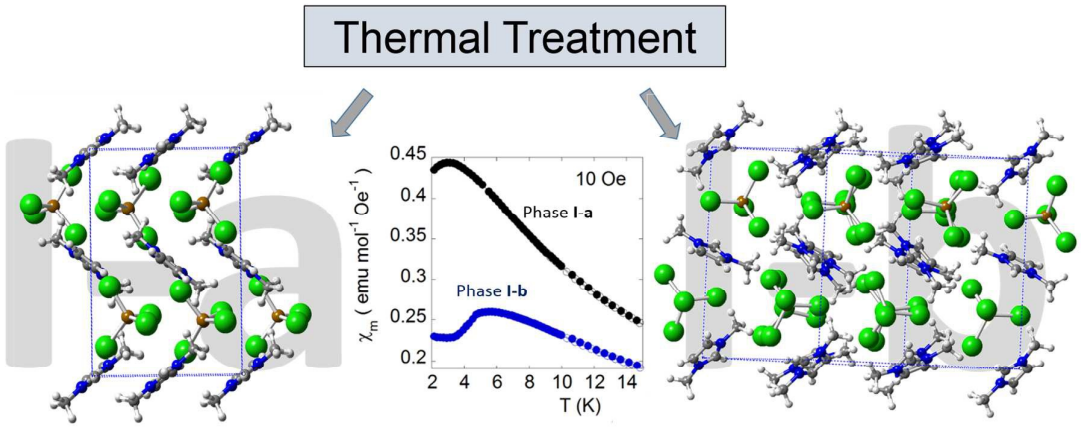

TOC

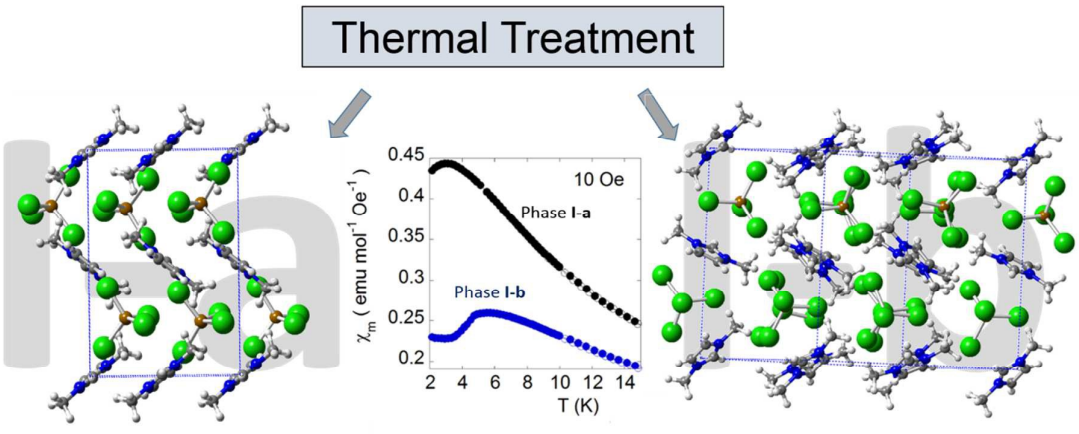

Synopsis: We present a solid-to-solid phase transition induced by thermal treatment in a Magnetic Ionic Liquid (MIL) which induces the modification of the magnetic properties and super-exchange pathways of the two low temperature phases obtained after the thermal treatment. A combination of several experimental methods: Synchrotron powder X-ray, Neutron powder diffraction, density functional theory, magnetometry, Mössbauer and Muon spectroscopy has been used in order to shed light to the different features observed.